1. Introduction

This work shows estimates of photometric nights from satellite-observed outgoing longwave radiation (OLR) and OLR anomalies for the Paranal and Chajnantor area.

More than 27 years of twice daily OLR measurements are available from NOAA satellites. These data are presented on a 2.5º x 2.5º global grid from July 1974 to September 2000, with a ten-month gap from March to December 1978. OLR data have been particularly useful for routine monitoring of cloudiness and rainfall over the tropics.

During the last two years, a decrease of photometric nights over the Paranal Observatory has been detected. Such a decrease of this important variable of the observatory's observing conditions can be explained by a sudden increase of cloudiness over the Atacama Desert. OLR data can give a clue of what is going on over this area.

Section 2 describes the concepts of atmospheric radiation. After developing the fundamental laws governing radiative transfer and radiative equilibrium it is shown how the incoming shortwave radiation and outgoing longwave radiation are the main components of the energy budget of earth. Since in a clear day more longwave radiation is emitted from earth than in a cloudy day, OLR can be considered as a good estimation of cloudiness.

Section 3 shows a description of the OLR data used for this study, how it has been previously used, and the methodology and criterion used to obtain photometric nights. To consider a night to be photometric, it must have at least 6 consecutive hours with a cloudless sky down to 18 degrees above horizon. Statistics of photometric nights at Paranal since the beginning of the VLT site survey have been collected from visual observations.

A 16-year comparison between monthly averages of photometric nights observed at Paranal and photometric nights obtained from OLR data and a 27-year study of night-time OLR data for the closest grid point to Paranal Observatory and Chajnantor are shown in section 4.

Section 5 presents the conclusions: despite the different definition between them, the photometric nights derived from OLR well captures the obtained from visual observations at Paranal. It also suggests a future work using the same OLR data and other NCEP/NCAR reanalysis data to estimate a possible displacement or enhancement of the Bolivian high over the Paranal area for the last two years.

2. Atmospheric radiation

2.1 Main concepts

Energy transfer in the atmosphere involves radiation in two distinct wavelength bands. Shortwave (SW) radiation emitted by the sun and longwave (LW) emitted by the earth's surface and atmosphere.

The spectrum of SW radiation, which is concentrated at wavelengths shorter than 4 µm, peaks in the visible near λ=0.5 µm. Tails of the SW spectrum extend into the Ultra violet (UV) and into the near infrared region ($0.2 < \lambda < 5$ µm). On the other hand, the LW spectrum peaks well into the Infra red (IR) at a wavelength of about 10 µm. Tails of the LW spectrum extend down to wavelengths of about 4 µm and out to 100 µm ($4 < \lambda < 100$ µm) (see figure 1). Overlap between the spectra of SW and LW radiation is negligible, so they may be treated independently by considering wavelengths shorter and longer than 4 µm. This can be seen on figure 1, where a blackbody radiation for 5780 K and 255 K are depicted.

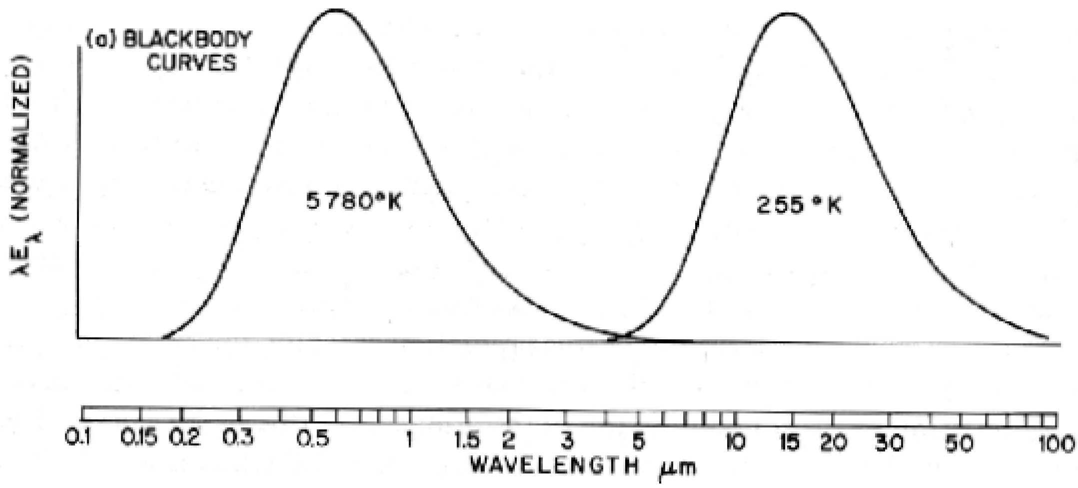

Figure 1: Normalized blackbody curves for 5780 K and 255 K, plotted so that irradiance is proportional to the areas under the curves (Wallace and Hobbs, [2]).

To maintain thermal equilibrium, a substance that absorbs radiant energy must also emit. Blackbody radiation is an idealization that corresponds to the energy emitted by an isolated cavity in thermal equilibrium. Such radiation is characterized by the following properties:

- The radiation is uniquely determined by the temperature of the emitter.
- For a given temperature, the radiant energy emitted is the maximum possible at all wavelengths.
- The radiation is isotropic; that is to say, it is independent of direction.

In addition to being a perfect emitter, a blackbody is also a perfect absorber: Radiation incident on a blackbody is completely absorbed at all wavelengths.

Planck postulated that the energy E of the molecules is quantized and can undergo changes only in discrete transitions that satisfy

$$\Delta E = \Delta n \cdot h\nu \qquad \text{Eq. 1}$$

where Δn is integer, h is Planck's constant and ν is the frequency of the electromagnetic radiation emitted or absorbed to accomplish the energy transition ΔE.

On this basis, Planck derived the following relationship between the spectrum intensity B_λ emitted by a population of molecules and their absolute temperature:

$$B_\lambda(T) = \frac{2hc^2}{\lambda^5 (e^{\frac{hc}{k\lambda T}} - 1)} \qquad \text{Eq. 2}$$

where k is the Boltzmann constant and c is the velocity of light. This spectrum possesses a single maximum at wavelength λ_m and increases with temperature.

According to the Wien's Displacement Law, the wavelength of maximum intensity follows from Eq. 2 as

$$\lambda_m = \frac{2897}{T} \quad [\mu m] \qquad \text{Eq. 3}$$

which decreases with increasing temperature of the emitter. Solar SW radiation incident on the top of the atmosphere is concentrated in the visible and peaks near 0.480 μm, corresponding to blue light. Wien's displacement law then implies an effective solar temperature of about 6000 K. On the other hand, the 288 K mean surface temperature of earth corresponds to maximum emission at a wavelength of about 10 μm.

The total flux F emitted by a blackbody at temperature T is obtained by integrating over the electromagnetic spectrum and is described by the Stefan-Boltzmann law as:

$$F = \sigma T^4 \qquad \text{Eq. 4}$$

where σ is the Stephan-Boltzmann constant ($\sigma = 5.67 \times 10^{-8}$ W m^{-2} K^{-4}) and F is in [W m^{-2}].

The preceding laws are determined for a substance that behaves as a blackbody. Real substances absorb and emit radiation at rates smaller than those of a perfect absorber and emitter. A graybody absorbs and emits with efficiencies that are independent of wavelength. The absorptivity a_λ of a substance is defined as the ratio of the intensity it absorbs to $B_\lambda(T)$. Similarly, emissivity ε_λ is defined as the ratio of intensity emitted by a substance to $B_\lambda(T)$.

For a graybody to be in equilibrium, the flux of energy it emits, $\varepsilon_\lambda \sigma T^4$, must equal the flux of energy it absorbs $a_\lambda \sigma T^4$. Applying this reasoning to substances of arbitrary monochromatic absorptivity and emissivity leads to the conclusion

$$\varepsilon_\lambda = a_\lambda \qquad \text{Eq. 5}$$

Known as the Kirchhoff's law, Eq. 5 asserts that a substance emits radiation at each wavelength as efficiently as it absorbs it. For LW radiation from the earth, emissivity ε_λ can be considered 0.9.

In general, the radiative efficiency of a substance varies with wavelength. For example, a surface like snow absorbs weakly in the visible but strongly in the IR. In the next section, we will discuss the case of SW radiation that passes freely through the atmosphere and then is absorbed at the surface, but the LW radiation reemitted by the surface, to preserve thermal equilibrium, is trapped by the overlaying atmosphere. To compensate the reduced transmission, the surface must emit more LW radiation, which requires a higher temperature, until the LW radiation rejected just balances the SW radiation absorbed. The increased surface temperature (e.g. greenhouse effect) is related directly to the difference in opacity between the visible and IR.

2.2. Radiative equilibrium

The driving force for the atmosphere is the absorption of solar energy at the earth's surface. Over timescales long compared to those controlling the redistribution of energy, the earth-atmosphere system is in thermal equilibrium, so the net energy gained must vanish. Consequently, absorption of solar SW radiation must be balanced by emission to space from the planet's surface and atmosphere, which is concentrated in the LW radiation.

The earth intercepts a beam of SW radiation, F_s. A fraction of the intercepted radiation, corresponding to the albedo α, is reflected back to space by the planet's surface and components of the atmosphere. The remainder of the incident SW flux: $(1-\alpha)$ F_s, is then absorbed by the earth-atmosphere system and distributed across the globe as it spins in the line of the beam. The global-mean albedo α is considered to be 0.3.

To maintain thermal equilibrium, the earth and atmosphere must re-emit to space LW radiation at exactly the same rate. Also referred to as *outgoing longwave radiation* (OLR), the emission to space of terrestrial radiation is described by the Stefan-Boltzmann law (Eq. 4).

The equivalent blackbody temperature T_e of the earth results of 255 K. This value is 33 K colder than the global-mean surface temperature, T_s=288 K.

The discrepancy between T_e and T_s follows from the atmosphere's different transmission characteristics of SW and LW. While SW passes freely to the earth's surface, where it can be absorbed, LW radiation emitted by the planet's surface is captured by the overlaying air. Energy absorbed in an atmospheric layer is then re-emitted, half upward and half downward. The upwelling radiation is absorbed again in overlaying layers, which subsequently re-emit that energy in similar way. The raise of the surface's temperature results from the fact that much of the outgoing longwave radiation is "trapped" by the atmosphere (due to the presence of water vapour, carbon dioxide, and clouds) and emitted back to the ground. In order to satisfy the radiation balance the surface must compensate by emitting more radiation than it would in the absence of such an atmosphere. To emit more it must radiate at a higher temperature. This atmospheric transmission characteristic of LW elevates the surface temperature of the earth, known as the *greenhouse effect*.

2.3 The global energy budget

The globally averaged energy budget is illustrated on Figure 2.

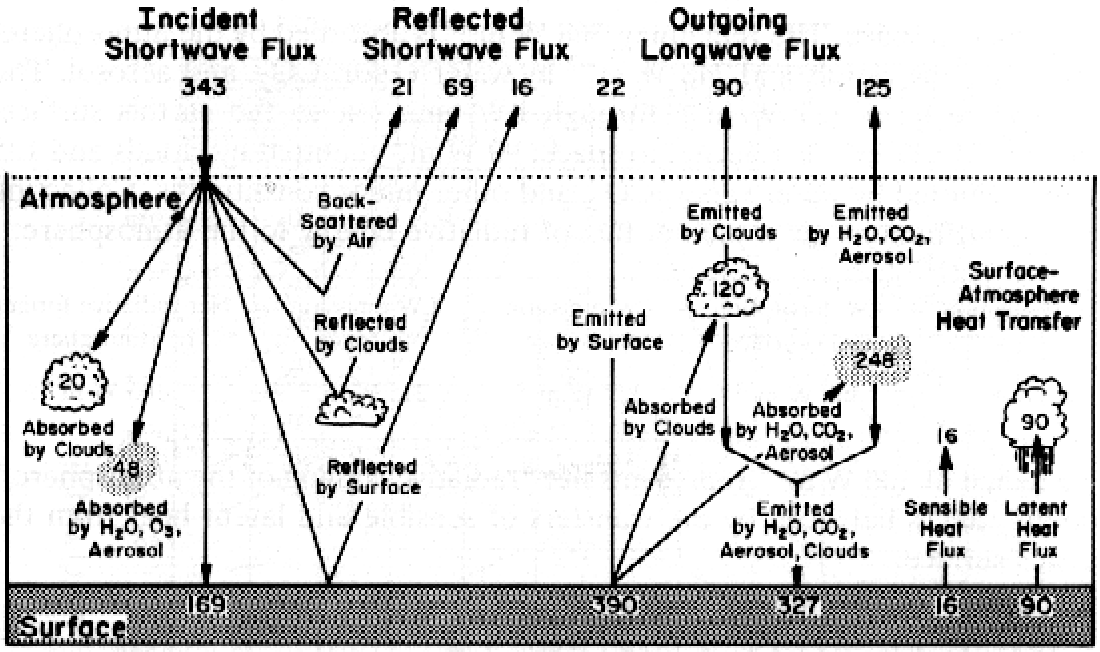

Figure 2: Global-mean energy budget (W m^{-2}). Made from recent satellite measurements of the earth's radiation budget (Salby, [1]).

Incoming solar energy is distributed across the earth. Therefore, the global-mean SW flux incident on the top of the atmosphere is given by F=343 W m^{-2}. Of this incident 343 W m^{-2}, a total of 106 W m^{-2} (approximately 30%) is reflected back to space: 21 W m^{-2} by air, 69 W m^{-2} by clouds, and 16 W m^{-2} by the surface. The remaining 237 W m^{-2} is absorbed in the earth-atmosphere system. Of this, 68 W m^{-2} (about 20% of the incident SW flux) is absorbed by the atmosphere: 48 W m^{-2} by atmospheric water vapour, ozone, and aerosol and 20 W m^{-2} by clouds. This leaves 169 W m^{-2} to be absorbed by the surface – nearly 50% of that incident on the top of the atmosphere.

The 169 W m^{-2} absorbed at the ground must be re-emitted to maintain thermal equilibrium of the earth's surface. At a global-mean surface temperature of 288 K, the surface emits 390 W m^{-2} of LW radiation according to Eq. 4 far more than it absorbs as SW radiation. Excess LW emission must be balanced by transfers of energy from other sources. Owing to the greenhouse effect, the surface also receives LW radiation that is emitted downward by the atmosphere in the amount 327 W m^{-2}. Collectively, these contributions result in a net transfer of radiate energy to the surface of 106 W m^{-2}.

The surplus of 106 W m^{-2} represents net "radiative heating of the surface". For equilibrium, this must be balanced by transfers of sensible and latent heat to the atmosphere.

Sensible heat transfer accounts for 16 W m^{-2} through conduction with the atmosphere. Latent heat transfer accounts for the remaining 90 W m^{-2}, which follows from evaporative cooling of the oceans. If it would not be by these supplemental forms of energy transfer, the earth's surface would have to be some 50 K warmer to balance the net absorption of radiant energy.

The energy budget of the atmosphere must also balance to zero to maintain thermal equilibrium. The atmosphere receives 68 W m^{-2} directly through absorption of SW radiation. Of the 390 W m^{-2} of LW radiation emitted by the earth's surface, only 22 W m^{-2} passes freely through the atmosphere and is rejected to space. The remaining 368 W m^{-2} is absorbed by the atmosphere: 120 W m^{-2} by clouds and 248 W m^{-2} by water vapour, CO_2, and aerosol. The atmosphere loses 327 W m^{-2} through LW emission to the earth's surface. Another 215 W m^{-2} is rejected to space: 90 W m^{-2} emitted by clouds and 125 W m^{-2} emitted by water vapour, CO_2, and other minor constitutents. Collecting these contributions gives the net flux of radiative energy to the atmosphere of 106 W m^{-2}.

The deficit of 106 W m^{-2} represents net "radiative cooling of the atmosphere", cooling that is balanced by the transfers of sensible and latent heat from the earth's surface.

From this global-mean energy budget (Fig. 1), it is seen that albedo is approximately 0.3 of the total incident SW; the total outgoing longwave radiation (OLR) is 237 W m^{-2}; and the net radiation, defined as the difference between the SW radiation absorbed and the LW radiation emitted by the earth-atmosphere system, is zero ((343-21-69-16) – (22+90+125) W m^{-2}).

Clouds routinely cover about 50% of the earth and account for about half of its albedo. Marine statocumulus are particularly important because they cover a large fraction of the globe and reflect much of the incident SW radiation. However, because their cloud-top temperatures do not differ substantially from those of the surface, marine stratocumulus do not appreciably modify OLR and hence the LW energy budget. In contrast, deep cumulus over Africa, South America, and the maritime continent have cloud-top temperatures as much as 100 K colder than the underlying surface, so they sharply reduce OLR from that under cloud-free conditions.

2.4 Horizontal distribution of radiative transfer

The previous section focused on vertical transfers associated with the global-mean energy balance. However, geometrical considerations, variations in optical properties, and cloud cover make radiant energy transfer nonuniform across the globe.

At low latitudes, SW radiation arrives nearly perpendicular to the earth with a higher flux of energy than at high latitudes, where SW radiation arrives at an oblique angle. The daily-averaged SW flux incident on the top of the atmosphere is referred to as the insolation that depends on the solar zenith angle, which is measured from local vertical, and on the length of the day.

Optical properties of the atmosphere also lead to a nonuniform heating of the planet. At low latitudes, SW radiation passes almost vertically through the atmosphere, so the distance traversed through absorbing constituents is minimized. At middle and high latitudes, SW radiation traverses the atmosphere that involves a much longer distance and therefore results in greater absorption.

Low latitudes are characterized by very low albedo and thus absorb most of the SW energy incident on them. High latitudes, particularly in the winter hemisphere, have extensive coverage by snow and ice, surfaces with a high albedo that reflects back to space much of the SW energy incident on them. Cloud cover adds to the high albedo of extratropical regions, for example, in the storm tracks. A high albedo is also evident in the tropics, where deep convection leads to maxima over the Amazon Basin, tropical Africa, and Indonesia.

Outgoing longwave radiation is dominated by the poleward decrease of temperature, which results in OLR decreasing steadily with latitude. Anomalously low OLR is found near the equator, over the convective centers of South America, Africa and Indonesia. High cloud tops in those regions have very low temperatures, so their LW emissions are substantially smaller than those from the surface in neighboring cloud-free regions. In fact, subtropical latitudes are marked by distinct maxima of OLR in regions flanking organized convection. Sinking motion there, which compensates rising motion inside the Inter Tropical Convergence Zone (ITCZ), inhibits cloud formation and precipitation, maintaining arid zones that typify the subtropics.

Although the global-mean net radiation must vanish for thermal equilibrium, this need not be the case locally. Low latitudes are characterized by a surplus of net radiation (warming) whereas high latitudes have a deficit of net radiation (cooling).

3. OLR Data

3.1 Description

Measurements by the two-channel scanning radiometer aboard the NOAA operational satellites were used to determine components of the earth-atmosphere radiation budget over the entire globe. The components consist of the outgoing longwave radiation, the albedo and the related absorbed solar radiation, and the net radiation.

The measuring instrument is a scanning radiometer flown aboard NOAA operational polar-orbiting satellites. These satellites are sun synchronous and orbit the earth at ~1500 km with a period of ~117 min. Equator crossing times have changed with the use of different satellites throughout the years (see figure 2). The radiometer senses energy in the visible (0.5-0.7 μm) portion of the spectrum and in the infrared window region (10.5-12.5 μm). The spatial resolution of the sensors are ~4 km for the visible and ~8 km for the infrared at the subsatellite point. The two infrared observations per day are corrected to a nadir view at the top of the atmosphere, and the visible observations are divided by cos ζ, where ζ is the solar zenith angle. In estimating the albedo and outgoing radiation, subsets of high resolution data are averaged and a 2.5º global grid data sets are produced. Values of the earth-atmosphere radiation balance parameters consist of daytime and nighttime observations.

The estimate of total longwave radiation flux from radiance measurements in the window region is made by use of a regression model that was derived from radiation calculations made for 99 different atmospheres covering a broad range of temperature and moisture as well as overcast and clear sky conditions [3].

Since the beginning of the NOAA outgoing longwave radiation data set in June 1974, there have been several changes in satellites, their orbits, and instrumentation [4]. Figure 3 shows a list of satellites used, with their initial equatorial crossing times.

Date	Satellite	Daytime crossing	Comments
74/6/1 – 78/3/16	SR series	09:00	
78/3/17 – 78/12/31			missing
79/1/1 – 80/1/31	Tiros N	15:30	
80/2/1 – 81/9/6	NOAA 6	07:30	
81/9/7 – 85/2/4	NOAA 7	14:30	
85/2/5 – 88/11/7	NOAA 9	14:30	
88/11/8 – 88/11/30	NOAA 10	07:30	
88/12/1 – 90/6/30	NOAA 11	14:30	
90/7/1 – 90/7/4	NOAA 10	07:30	4 days only
90/7/5 – 91/3/4	NOAA 11	14:30	
91/3/5 – 91/3/5	NOAA 10	07:30	1 day only
91/3/6 – 91/3/12	NOAA 11	14:30	
91/3/13 – 91/3/13	NOAA 10	07:30	1 day only
91/3/14 – 91/8/13	NOAA 11	14:30	
91/8/14 – 91/8/14	NOAA 10	07:30	1 day only

91/8/15 – 92/10/14	NOAA 11	14:30	
92/10/15 – 92/10/15	NOAA 12	07:30	1 day only
92/10/16 – 94/9/16	NOAA 11	14:30	
94/9/17 – 95/1/31	NOAA 12	07:30	
95/2/1 – 99/5/27	NOAA 14	14:30	

Figure 3: List of satellites used with their initial equatorial crossing times. The 14:30 crossing times are preferred being available for the longest time. Changing crossing times can cause spurious variability, especially over land. Source: NCAR/NOAA

3.2 Previous studies that used OLR

The OLR dataset have been used extensively in meteorological studies, both as one component of the radiation balance of the atmosphere and to infer changes in the amount and height of clouds. In particular, the dominant role of clouds in determining OLR over the tropics has led to extensive use of it as an indicator of convective activity, and its broad spatial coverage and long record period have made it valuable in investigating atmospheric phenomena with a wide range of temporal and spatial scales [6].

In the Tropics, where surface temperatures vary modestly through the annual cycle, the strongest variations in OLR result from changes in the amount and depth of clouds. This direct physical connection with clouds led to the use of OLR in quantitative precipitation estimation beginning in the early 1980s. The first published work of this sort was by Lau and Chan [7], in which the number of days in a month with OLR less than 240 W m^{-2} was used as a predictor of monthly precipitation and calibrated against estimates based on microwave observations over Tropical oceans. Morrissey [8] analyzed the relationships among the OLR, precipitation, and moisture budget over the tropical Pacific and found that daily OLR correlates negatively and significantly with precipitation over the tropical areas where deep convection dominates.

These techniques are not applicable to extratropical areas where variations in surface temperatures are as important or more important than cloudiness in determining the magnitude of the total OLR flux [6]. However, Susskind et al [9] have shown that monthly anomalies in OLR are correlated positively with surface temperature over land and negatively with cloudiness over the ocean in mid and high latitudes. Since continental temperature anomalies are often correlated with precipitation, and since total cloud cover might be expected to exhibit a positive correlation with precipitation, it seems worth to investigate the relationship between OLR and precipitation globally.

Lau and Chan [7] obtained frequency distributions for convective clouds study. They used daily data to keep track of the total number of days within a given month at each grid point in which the daily-averaged OLR value fell below a threshold value. The threshold criterion is interpreted to mean that the cloud associated with deep convection has reached a certain fixed height in the upper troposphere. This yield, for each month period, a frequency count N_c in number of days per month. Different values of the threshold were tested and the results were not very sensitive to the exact value of the threshold used, given to be within the 230-250 W m^{-2} range.

A similar method than the used by Lau and Chan [7] to obtain N_c is used in this work. A monthly fraction (number of photometric nights per month divided by the number of days of that month) is used to estimate photometric nights at Paranal and Chajnantor. The threshold criterion to consider a non-photometric night is explained in section 3.4.

3.3 Photometric nights

Statistics of photometric nights at Paranal since the beginning of the VLT site survey and at La Silla Observatory (29.25º S, 70.73º W, 2400 m.a.s.l) are available at the Paranal web page. Data is collected from visual observations at Paranal and extracted from the telescope observing logs at La Silla. A photometric night must have at least 6 consecutive hours with a cloudless sky down to 18 degrees above horizon. Monthly average fraction of photometric nights at Paranal and La Silla is plotted on Figure 4. The mean value for Paranal is 0.78 and for La Silla is 0.61 for the period between 1983-2000.

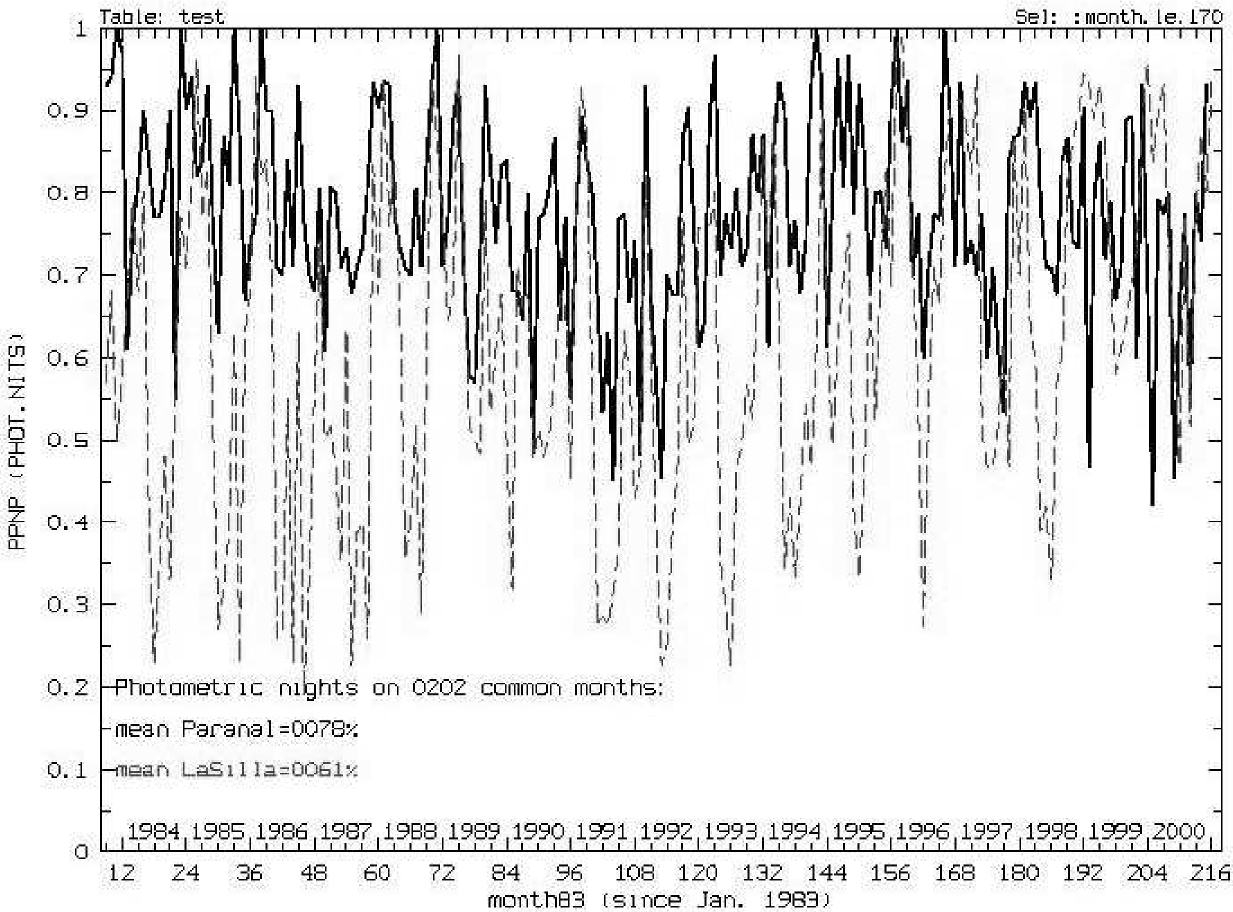

Figure 4: Statistics of photometric night since June 1983 to the present for Paranal (black) and La Silla (red).

3.4 Methodology

For this work, three types of data were used. The primary data used consists of nearly 27 years of twice-daily estimates of outgoing longwave radiation from the National Oceanic and Atmospheric (NOAA) polar orbiting satellites extending from June 1974 to September 2000, with a 10 month gap in 1978. The two observations per day are a mapping of the daytime and nighttime passes of the satellite to the synoptic times of 06:00 and 18:00 UTC (02:00 and 14:00 Paranal winter local time). Such a mapping is accurate to within 6 h and is done in such a way that each synoptic grid contains half daytime and half nighttime data [10]. Before the mapping to synoptic times, the daytime and nighttime passes were independently interpolated in space and time to remove any missing values [5]. The data from each scanning swath of the satellite are archived on a 2.5º grid. We are only interested in the closest grid point (25º S, 70º W, and 1843 m.a.s.l) to Paranal and (22.5º S, 67.5º W, and 4029 m.a.s.l) to Chajnantor. This twice daily OLR data for both grid points was personally received from Brant Liebmann (NOAA-CIRES Climate Diagnostics Center).

The second data set used is the NCEP/NCAR Reanalysis (Kalnay et al. [11]) surface air temperature for the closest grid point to Paranal and Chajnantor, which are the same grid points used for OLR. Both datasets start from 1974 to the present and are given at 00:00, 06:00, 12:00, and 18:00 UTC. The value that corresponds to 06:00 UTC is used to represent night temperatures. Similar datasets were also used in a previous work of Bustos for 52 years of climatological data for the Paranal and Chajnantor area and it proved to be close to the observed temperatures on both sites [12, 13, 14].

In order to obtain a photometric or non-photometric night value, the OLR data is first converted to temperature using Eq. 4. Then, NCEP/NCAR Reanalysis surface air temperature of that night (06:00 UTC) is subtracted in order to obtain anomalies. If negative anomalies are larger than 2.4 K, that night is considered a non-photometric night. Then, the number of non-photometric nights in a month is counted to obtain the percentage of photometric nights for that month. The 2.4 K represents the threshold value that gives the same average for the observed and OLR estimated photometric nights for the complete 1984-2000 period, which is 0.778.

Finally, to compare photometric nights that are derived from the previous datasets (OLR and NCEP/NCAR surface air temperature), data of observed photometric nights from Paranal Observatory since 1984 is available on the Web pages maintained by Marc Sarazin.

4. Cross-correlation and 27 years of OLR data

4.1 Cross-correlation of photometric nights

A cross-correlation analysis between the observed photometric nights at Paranal with the obtained from OLR data is depicted on figure 5.

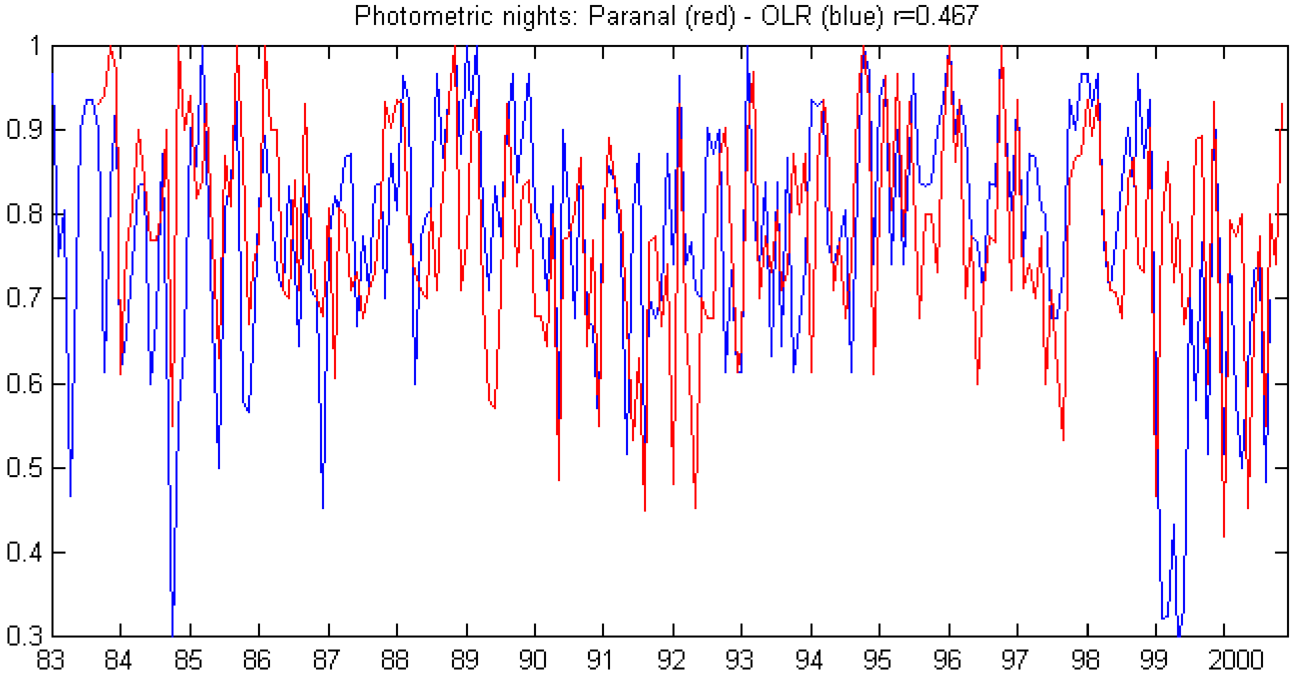

Figure 5: Photometric nights observed at Paranal (red) and the obtained from OLR satellite-observations (blue).

It is seen that photometric nights obtained from OLR well follows the observed at Paranal with a 7-year cycle observed in both datasets. A cross-correlation value of r = 0.467 is obtained. One reason to obtain such a relative low cross-correlation value is due to the different definition of photometric nights for both datasets. Since Paranal observations consider 6 consecutive hours of a cloudless sky, nightly OLR data is obtained from a single satellite observation at a specific time (see figure 3). It has to be considered that the OLR data is transformed to temperature and then is subtracted to a single nightly observation (06:00 UTC) of NCEP/NCAR reanalysis surface temperature for the same grid point to obtain nightly anomalies that are counted to obtain statistics of photometric nights. Another reason to obtain this low value is that the definition of photometric nights introduces a decision criterion in a binary representation, which is different for both cases.

A scatter diagram between measured photometric nights and OLR derived data for the Paranal area is shown on figure 6. A linear fit of least-squares gives a slope of 0.5475 and a constant of 0.3515.

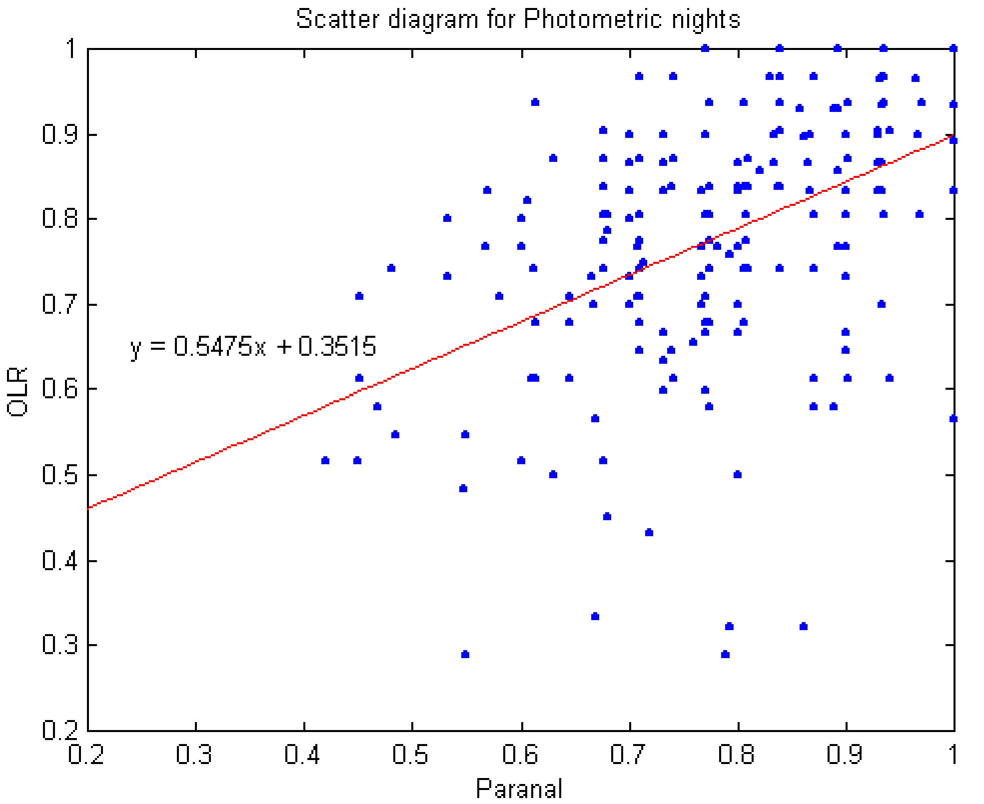

Figure 6: Scatter diagram for Paranal observed and OLR estimated photometric nights.

Figure 7 shows the photometric night's annual cycle for the complete 27-year period for Paranal and Chajnantor (see section 4.3) and the annual cycle obtained for the observed photometric nights at Paranal for the 18-year period. Both annual cycles at Paranal present similar patterns. The photometric night's annual cycle for the OLR estimated at Paranal shows a maximum monthly average on February of 0.8733 and a minimum on May of 0.7445.

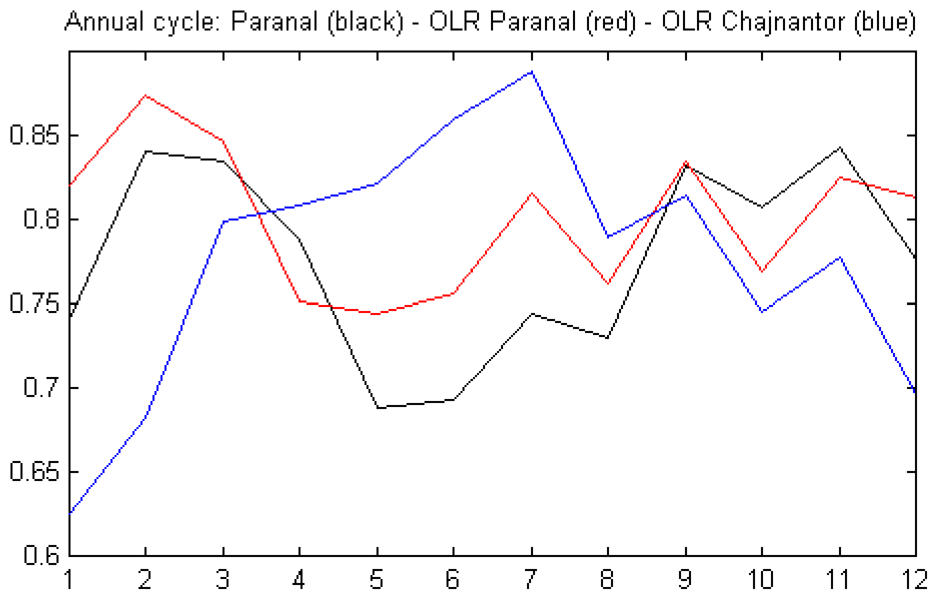

Figure 7: Annual cycle of photometric nights observed at Paranal and the obtained from OLR at Paranal and Chajnantor. A maximum in February for Paranal and July for Chajnantor is observed.

4.2 27 years of OLR data for the Paranal area

According to the previous results, it is possible to obtain an estimation of the photometric nights for the Paranal area using the same criterion than in 4.1 for the 1974-2000 period. Figure 8 shows the complete series of photometric nights derived from OLR. This OLR data is referred to a grid point located ~60 Km south-east and ~800 m lower in altitude than Paranal [12].

As on Figure 5, it is clearly seen a 7-year cycle with another cycle of 4.25 years. In October 1998, a very significant decrease of photometric nights is observed with a negative tendency. The best observing conditions (over 0.85) for the complete period are obtained during the years 1974-1978, 1980-1981, 1988-1989, 1995-1996, and 1998. The poorest observing conditions (below 0.75) are obtained in the years 1979, 1984, 1986, 1990-1991, 1993, and 1999-2000. These cycles of about 7 years have the most positive anomaly during the years 1976-1977 and the most negative anomalies during the last years 1999-2000.

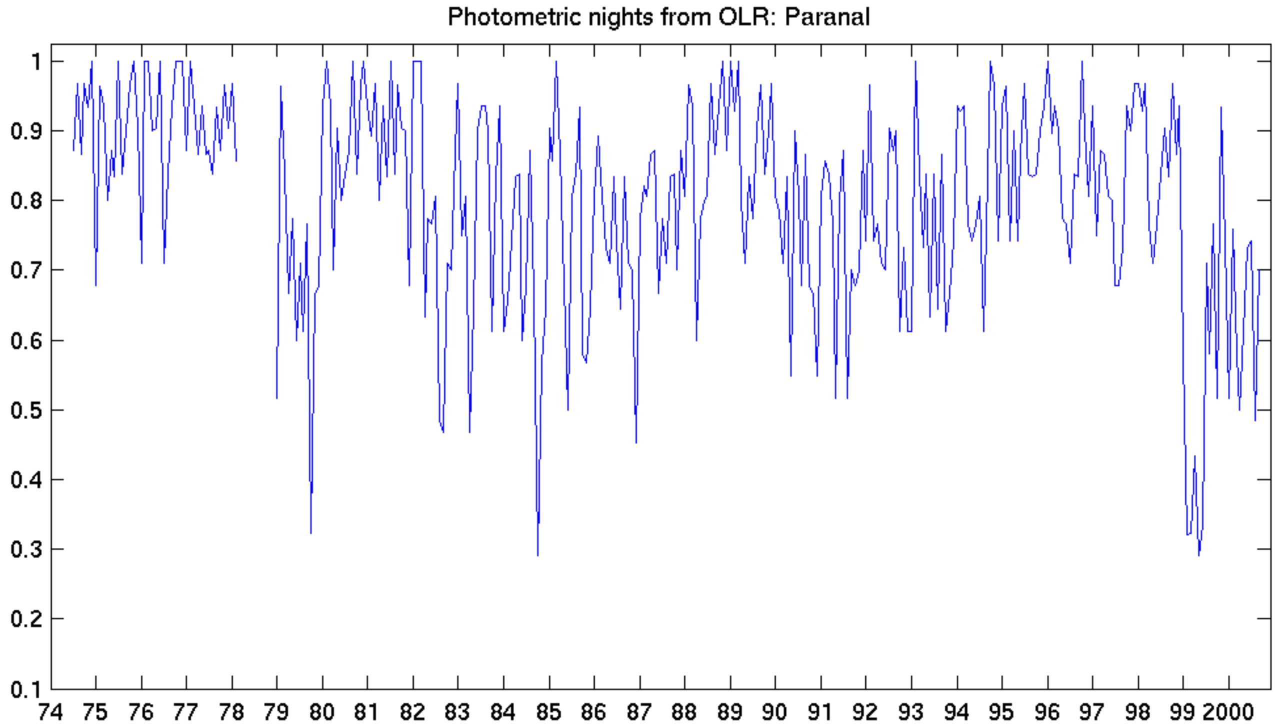

Figure 8: Photometric nights obtained from OLR satellite-data for the 1974-2000 period, with a 10-month gap in 1978 for the Paranal area.

The mean value of photometric nights obtained for the complete 1974-2000 period is 0.8012, slightly higher than the 0.778 previously obtained for the 1983-2000 period.

4.3 27 years of OLR data for the Chajnantor area

In the same way that it was done for the Paranal area, it is possible to estimate 27 years of photometric nights for the Chajnantor area. Due to the lack of photometric night's observations on Chajnantor, it is not possible to compare the OLR data with on-site observations. Using the same threshold value of 2.4 K used for the Paranal area, the complete series of photometric night for Chajnantor is shown on figure 9. This OLR data is referred to a grid point located ~60 Km north and ~1000 m lower in altitude than Chajnantor [14].

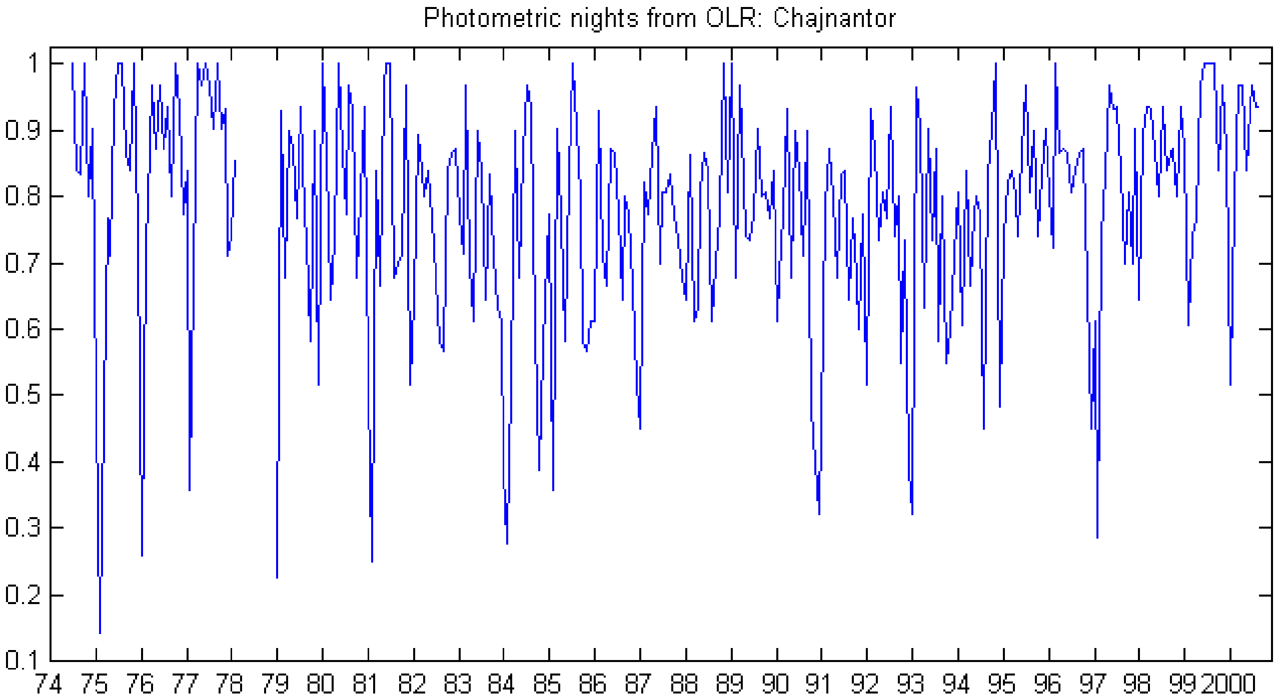

Figure 9: Photometric nights obtained from OLR satellite-data for the 1974-2000 period, with a 10-month gap in 1978 for the Chajnantor area.

The 7-year cycle is also found in this series. The best years (above 0.85) are during the years 1974, 1977, 1980, and 1998-2000 while the poorest years (below 0.75) are during the years 1975, 1979, 1981, 1983-1986, and 1990-1994. For the last two years, a decrease of photometric nights is not found.

It is clearly seen that in the summer months (January and February) photometric nights decrease at the Chajnantor area due to the presence of the Bolivian High (Bolivian winter) over the Altiplano that produce convective clouds, storms and rain. The total average of the photometric nights obtained for the complete 1974-2000 period is 0.7754. If the summer months (January and February) are not considered, then the total average raises to 0.8004. July presents an average of 0.8883 (highest) and January has an average of 0.6253 (lowest).

On figure 7, it is shown that the annual cycle is the opposite as the obtained for Paranal, with austral winter months having better observing conditions than austral summer months. Moreover, these austral winter months (especially July) at Chajnantor have in average more photometric nights than summer months (February) in Paranal, though the total annual average (0.7754) is lower than in Paranal (0.8012).

4.4 OLR and temperature anomalies

Using the same NCEP/NCAR surface temperature data than in the previous work of Bustos [12, 13] for the same grid point it is possible to compare the behaviour of both OLR and temperature anomalies for the same 27-year period. This can be seen on figure 10, where Paranal observed temperature anomalies are also compared. Anomalies are obtained subtracting the data with the climatology that is to say, subtracting the averaged annual cycle for the 27-year period.

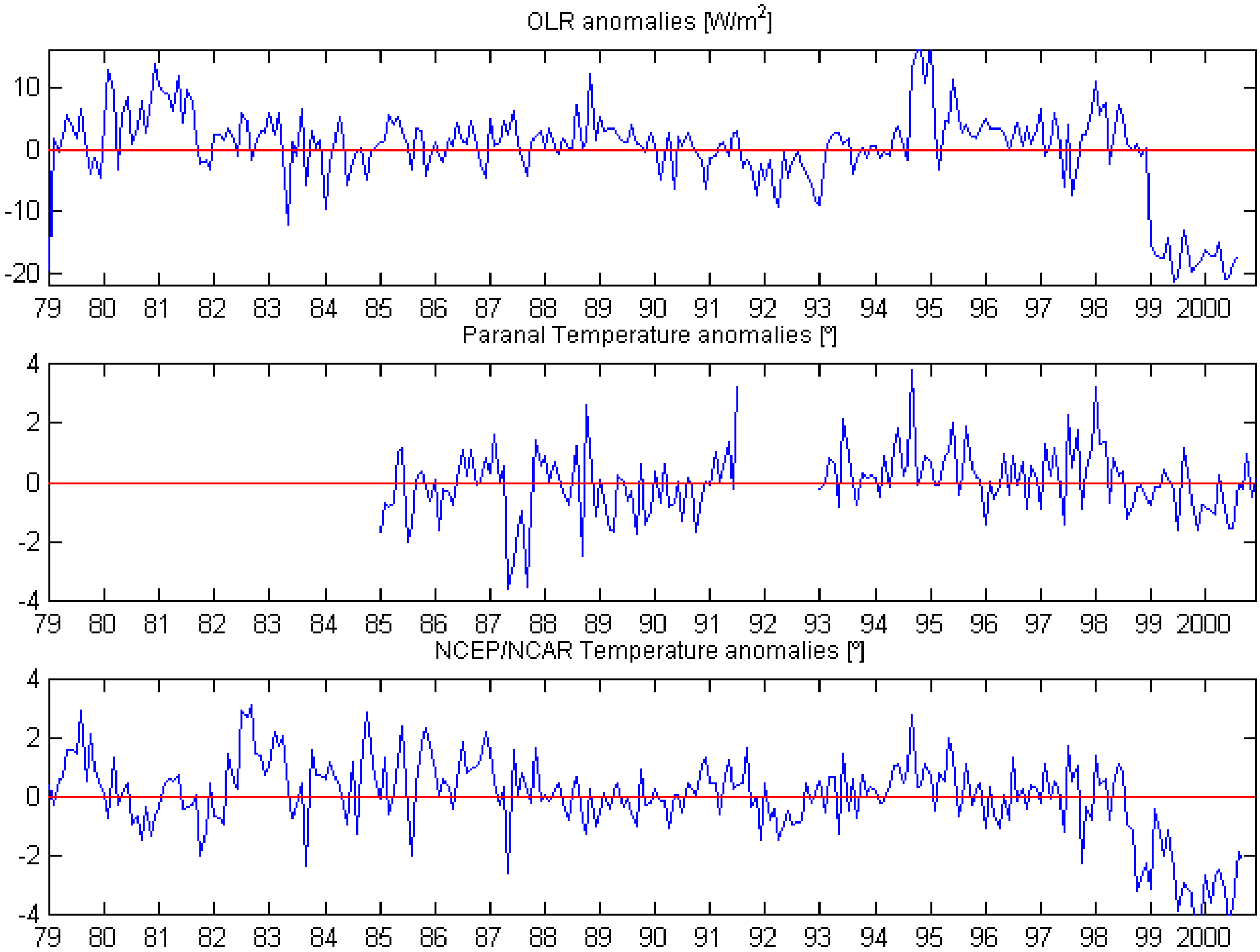

Figure 10: Anomalies for OLR, Paranal temperature and NCEP/NCAR surface temperature.

The strong 1999-2000 negative OLR anomaly was never been observed before as well as the negative NCEP/NCAR temperature anomaly. Both features can indicate an anomalous presence of the Bolivian high over the Paranal area. It is also interesting to see a 3-month delay between NCEP/NCAR temperature and OLR anomalies in 1998.

A 7-year cycle is also obtained for the OLR anomalies. For the case of NCEP/NCAR temperature anomalies, cycles of 3.67 years related to El Niño phenomenon are found.

5. Conclusions and future work

The results obtained from the cross-correlation analysis indicate that OLR data can be considered as a good estimate of observed photometric nights for the Paranal area, in spite of the fact that both come from different definitions as is described in 4.1.

An annual cycle (figure 7) of photometric nights is well defined for the Paranal area, with a maximum in austral summers and a minimum in austral winters. However, an opposite annual cycle behaviour is found for the Chajnantor area.

A 7-year cycle for both observed and OLR derived photometric nights for the Paranal area is found.

For the total period from 1974 to 2000, a mean value of photometric nights derived from OLR of 0.8012 is obtained for the Paranal area, slightly higher than the 0.778 average measured for the 1983-2000 period. For the Chajnantor area, a mean value of 0.7754 is found, but during austral summer months this value decrease down to near 0.65.

No evidences are found of spurious variability in OLR due to the change of satellite crossing times due to several changes in satellites, orbits, and instrumentation throughout the complete 1974-2000 observed period. For the case of the OLR drop in November 1998, no significant satellite change has been reported.

A delay of 3 months (figure 10) between the decrease of NCEP/NCAR surface air temperature and OLR is found for the Paranal area. While the NCEP/NCAR temperature drop begins in August 1998, the OLR start to fall in November of the same year.

The significant drop in OLR and temperature (figure 10) that affects photometric nights (figure 8) for the last two years at the Paranal area has not been experienced before. An enhancement or a south-west displacement of the Bolivian high to the Paranal area can be a reason. Moreover, the Chajnantor area does not show this drop of photometric nights because it has always been inside the convective zone.

A deeper study of the NCEP/NCAR reanalysis data of high troposphere pressure, winds and humidity for this area is needed to determine whether this change of the Bolivian high is really occurring and affecting the observing conditions at the Paranal site.

Acknowledgments

Twice-daily OLR data provided by Brant Liebmann of NOAA-CIRES Climate Diagnostics Center, Boulder, Colorado, USA. NCEP Reanalysis data provided by the NOAA-CIRES Climate Diagnostics Center, Boulder, Colorado, USA, from their Web site at http://www.cdc.noaa.gov/. Paranal meteorological data provided by Marc Sarazin (European Southern Observatory / Paranal Observatory).

Thanks are also given to Marc Sarazin for his comments and to Dr. Guillermo Delgado (Onsala Space Observatory / European Southern Observatory) for the review of this manuscript.

References

[1] Salby, M. L., 1996: "Fundamentals of Atmospheric Physics". Academic Press, San Diego.

[2] Wallace, J., and P. Hobbs, 1977: "Atmospheric Science: An introductory survey". Academic Press, San Diego.

[3] Gruber, A., and J. Winston, 1978: "Earth-atmosphere radiative heating based on NOAA scanning radiometer measurements". *Bull. Amer. Meteor. Soc.*, **59**, 1570-1573.

[4] Gruber, A., and A. Krueger, 1984: "The status of the NOAA outgoing longwave radiation data set". *Bull. Amer. Meteor. Soc.*, **65**, 958-962.

[5] Liebmann, B., and C. Smith, 1996: "Description of a complete (interpolated) outgoing longwave radiation dataset". *Bull. Amer. Meteor. Soc.*, **77**, 1275-1277.

[6] Xie, P., and P. Arkin, 1998: "Global monthly precipitation estimates from satellite-observed outgoing longwave radiation". *J. Climate*, **11**, 137-164.

[7] Lau, K., and P. Chan, 1983: "Short-term climate variability and atmospheric teleconnections from satellite-observed outgoing longwave radiation. I: Simultaneous relationships". *J. Atmos. Sci.*, **40**, 2735-2750.

[8] Morrisey, M., 1986: "A statistical analysis of the relationships among rainfall, outgoing longwave radiation, and the moisture budget during January-March 1979". *Mon. Wea. Rev.*, **114**, 931-942.

[9] Susskind, J., P. Piraino, L. Iredell, and A. Mehta, 1997: "Characteristics of the TOVS Pathfinder Path A dataset". *Bull. Amer. Meteor. Soc*., **78**, 1449-1472.

[10] Wheeler, M., and G. Kiladis, 1999: "Convectively coupled equatorial waves: Analysis of clouds and temperatures in the wavenumber-frequency domain". *J. Atmos. Sci.*, **56**, 374-399.

[11] Kalnay, E., and Coauthors, 1996: "The NCEP/NCAR 40-year reanalysis project". *Bull. Amer. Meteor. Soc.*, **77**, 437-471.

[12] Bustos, R., 2000: "A 52-Year Climatological Study for the Paranal Area Using NCEP/NCAR Reanalysis Data". Internal report, *European Southern Observatory*, Paranal Observatory.

[13] Bustos, R., 2001: "A 15-year cross-correlation analysis of NCEP/NCAR Reanalysis data with Paranal ground stations". Internal report, *European Southern Observatory*, Paranal Observatory.

[14] Bustos, R., G. Delgado, L. Nyman, and S. Radford, 2000: "52 years of climatological data for the Chajnantor area". ALMA Memo Series No. 333.

OLR study for the Paranal and Chajnantor area

Ricardo Bustos Placencia
Civil Electrical Engineer
University of Chile
rbustos@dgf.uchile.cl

Presented to the European Southern Observatory
Paranal Observatory

March 2001

Index

1. Introduction

2. Atmospheric radiation

2.1 Main concepts
2.2 Radiative equilibrium
2.3 The global energy budget
2.4 Horizontal distribution of radiative transfer

3. OLR data

3.1 Description
3.2 Previous studies that used OLR
3.3 Photometric nights
3.4 Methodology

4. Cross-correlation and 27 years of OLR data

4.1 Cross-correlation of photometric nights
4.2 27 years of OLR data for the Paranal area
4.3 27 years of OLR data for the Chajnantor area
4.4 OLR and temperature anomalies

5. Conclusions and future work

Acknowledgements

References